articles

Substrate-induced transmembrane signaling in the cobalamin transporter BtuB

David P. Chimento[1,2], Arun K. Mohanty[1,3], Robert J. Kadner[2] and Michael C. Wiener[3]

The outer membranes of Gram-negative bacteria possess transport proteins essential for uptake of scarce nutrients. In TonB-dependent transporters, a conserved sequence of seven residues, the Ton box, faces the periplasm and interacts with the inner membrane TonB protein to energize an active transport cycle. A critical mechanistic step is the structural change in the Ton box of the transporter upon substrate binding; this essential transmembrane signaling event increases the affinity of the transporter for TonB and enables active transport to proceed. We have solved crystal structures of BtuB, the outer membrane cobalamin transporter from *Escherichia coli*, in the absence and presence of cyanocobalamin (vitamin B$_{12}$). In these structures, the Ton box is ordered and undergoes a conformational change in the presence of bound substrate. Calcium has been implicated as a necessary factor for the high-affinity binding (K_d ~0.3 nM) of cyanocobalamin to BtuB. We observe two bound calcium ions that order three extracellular loops of BtuB, thus providing a direct (and unusual) structural role for calcium.

All organisms require organometallic cofactors, such as hemes, porphyrins and cobalamins, and must obtain them (or their precursors) from external sources. Gram-negative bacteria possess specialized systems that bind and transport these essential molecules across two membranes (outer and inner) and the periplasmic space for subsequent utilization within the cytosol. Specific outer membrane transporters bind their respective substrates in an energy-independent fashion[1]. Following the binding event, energy-dependent transport occurs across the outer membrane. The outer membrane does not maintain an electrochemical gradient. The energy required for transport is obtained by coupling the outer membrane transporter to the inner membrane in a manner enabling utilization of the protonmotive force of the inner membrane. Many of these bacterial outer membrane transporters are coupled with the TonB protein, which is part of an inner membrane complex that transduces energy to drive active transport[2–4]. The ubiquity of TonB-dependent outer membrane transport in Gram-negative bacteria presages this system as a potential target for the design of new antibiotics. TonB-dependent transporters possess a highly conserved stretch of seven amino acid residues, the Ton box, near their N termini[5,6]. Mutations in the Ton box of many outer membrane transporters cause a loss of TonB-dependent functions with no accompanying loss of other cellular function[7–9]. Thus, a key aspect of transmembrane signaling in the TonB-dependent transport cycle entails structural and/or dynamical changes in the Ton box of the transporter upon substrate binding. The X-ray crystal structures of three TonB-dependent iron-siderophore transporters, FepA, FhuA and FecA, have been solved[10–13]. Two of these, FhuA and FecA, have been solved both in the absence and presence of bound substrate. The structure of FepA without its siderophore substrate contains an ordered Ton box region. Unfortunately, the FhuA and FecA structures do not contain an ordered Ton box; thus, the structural behavior of this functionally critical 'coupling region' in the presence of substrate is unknown.

Numerous enzymes require cobalamin as a cofactor. In enteric bacteria, cobalamin-containing enzymes function in amino acid synthesis, nucleotide synthesis and metabolism[14]. Methylcobalamin is the cofactor for methionine synthetase, the enzyme that catalyzes the terminal step of methionine biosynthesis. Cyanocobalamin (vitamin B$_{12}$), or a product related to it, is involved in the synthesis by epoxyqueuosine reductase of the modified base queuosine, present in the anticodon loop of some tRNAs. Adenosylcobalamin is the cofactor for ethanolamine ammonia lyase, which catalyzes the first step in the catabolism of ethanolamine as a nitrogen or carbon source. All of these various cobalamins can be obtained or produced by bacteria after uptake of cyanocobalamin (vitamin B$_{12}$). The TonB-dependent outer membrane transporter for cobalamin in *Escherichia coli* is BtuB[7]. As assayed in outer-membrane preparations, cyanocobalamin binds to BtuB with high affinity (K_d ~0.3 nM) in the presence of calcium; depletion of calcium reduces this affinity 50–100 fold[15]. In addition to binding and transport of cobalamins, BtuB serves as a receptor for the E and A colicins and for bacteriophage BF23 (refs. 16,17). The elucidation of structures of the outer membrane transporter (BtuB, this paper), the inner membrane ABC transporter (BtuCD)[18] and the periplasmic binding protein (BtuF)[19] make cobalamin transport in *E. coli* the best structurally characterized transport system thus far. Here, we have determined four structures of BtuB: an initial methionine-substitution mutant used for experimental phase determination, the wild type protein, wild type protein with bound calcium, and wild type protein with bound calcium and cyanocobalamin (vitamin B$_{12}$). These structures, the first of an outer membrane transporter with a substrate that is not an iron siderophore, reveal several novel and interesting features. Among these features are a direct structural role for calcium in high-affinity substrate binding and a conformational change in the Ton box upon substrate binding. These structures are part of our ongoing efforts to dissect the molecular basis of TonB-dependent outer membrane transport.

[1]These authors contributed equally to the work. [2]Department of Microbiology and [3]Department of Molecular Physiology and Biological Physics, University of Virginia, Charlottesville, Virginia 22908, USA.

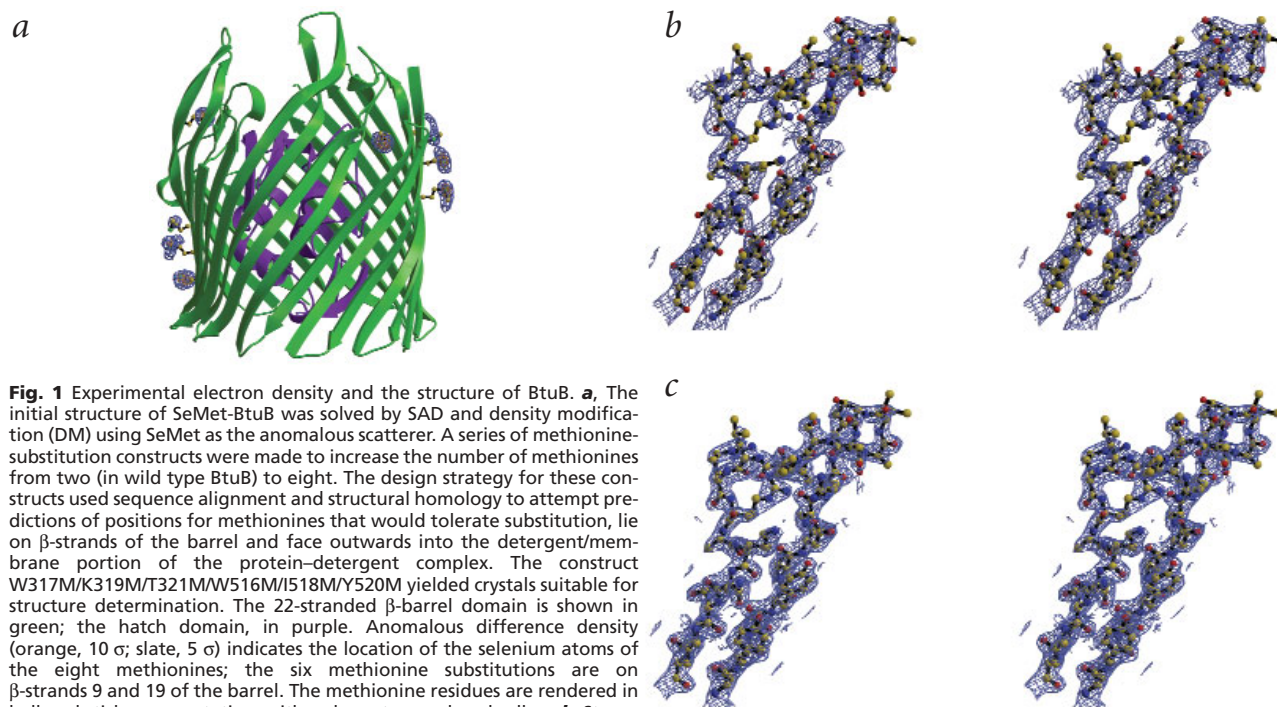Correspondence should be addressed to M.C.W. *e-mail: mwiener@virginia.edu*

Fig. 1 Experimental electron density and the structure of BtuB. ***a***, The initial structure of SeMet-BtuB was solved by SAD and density modification (DM) using SeMet as the anomalous scatterer. A series of methionine-substitution constructs were made to increase the number of methionines from two (in wild type BtuB) to eight. The design strategy for these constructs used sequence alignment and structural homology to attempt predictions of positions for methionines that would tolerate substitution, lie on β-strands of the barrel and face outwards into the detergent/membrane portion of the protein–detergent complex. The construct W317M/K319M/T321M/W516M/I518M/Y520M yielded crystals suitable for structure determination. The 22-stranded β-barrel domain is shown in green; the hatch domain, in purple. Anomalous difference density (orange, 10 σ; slate, 5 σ) indicates the location of the selenium atoms of the eight methionines; the six methionine substitutions are on β-strands 9 and 19 of the barrel. The methionine residues are rendered in ball-and-stick representation, with carbon atoms colored yellow. ***b***, Stereo view of experimental (2.7 Å resolution) FOM-weighted SAD-DM electron density (slate, 1.2 σ) for residues 480–504. This region of the SeMet-BtuB structure includes portions of the β-barrel strands 17 and 18, along with a long extracellular connecting loop. ***c***, Stereo view of σ_A[42]-weighted $2F_o - F_c$ electron density (slate, 1.5 σ) for this same region in apo BtuB structure (2.0 Å resolution). All figures prepared with MolScript[46], BobScript[47], Raster3D[48] and GRASP[49].

Overall structure

The initial structure of selenomethionine (SeMet)-containing BtuB, SeMet-BtuB, was solved by SAD phasing and density modification. Because the 594-residue wild type BtuB protein contains only two native methionines, a set of mutants each with six additional methionine substitutions was constructed. One of these mutants, W317M/K319M/T321M/W516M/ I518M/Y520M, yielded crystals suitable for structure determination (Fig. 1*a,b*). This 2.7 Å resolution structure, after partial refinement, was used in molecular replacement to solve the structure of a related crystal form of wild type protein (apo BtuB) for which a 2.0 Å resolution data set had been obtained (Fig. 1*c*). The structure of the ternary complex of BtuB, calcium and B_{12} (Ca^{2+}–B_{12}–BtuB) was solved to 3.1 Å resolution by molecular replacement with apo BtuB as the search model, in combination with experimental phase information provided by SAD data collected at the cobalt K-edge (λ = 1.6037 Å). The structure of the binary complex of BtuB and calcium (Ca^{2+}–BtuB) was solved to 3.3 Å resolution by molecular replacement with apo BtuB as the search model.

The basic modular architecture of the cobalamin transporter BtuB is similar to that of the iron siderophore transporters FepA[12], FhuA[10,11] and FecA[13]; specifically, an N-terminal hatch domain is embedded within the lumen of a 22-stranded β-barrel (Fig. 2). Following nomenclature used in the description of the structure of FhuA[11], we refer to the extracellular connections between contiguous strands of the barrel as 'loops' and the periplasmic connections between contiguous strands of the barrel as 'turns'. We refer to these loops (or turns) by the pairs of strands that they connect (for example, the 3–4 loop connects

β-strands 3 and 4 at the extracellular side of the barrel). In BtuB, the ordered portion of the hatch extends from residues 6–132, with the Ton box located at residues 6–12. The hatch is built around a core four-stranded β-sheet tilted at an angle of ~30–40° with respect to the membrane plane of the transporter. This core domain, defining the fold of the hatch, is conserved among the structures of outer membrane iron-siderophore transporters solved so far[10–13]. Most of the remainder of the hatch possesses no regular secondary structure, except for several short helices and strands. Four loops that connect secondary structural elements face the extracellular side of the β-barrel lumen. A linker of four residues connects the hatch to the first β-strand of the barrel (which begins at residue 137). The loops (and turns) that connect the 22 strands of the β-barrel domain display a conspicuous asymmetry in length between the loops on the extracellular side of the barrel (13.3 ± 6.1 residues) and the turns on the periplasmic side (3.0 ± 0.9 residues). The barrel domain has an elliptical cross-section of ~40 Å × 45 Å and a maximum height of 55 Å. BtuB is ~60–100 residues shorter in length than the iron-siderophore transporters solved so far. BtuB has a more squat structure, possessing shorter extracellular loops and containing a smaller hatch domain than these other transporters.

Ton box conformation

The structure of the Ton box in the Ca^{2+}–B_{12}–BtuB structure is significantly different from that in the Ca^{2+}–BtuB structure, as indicated from their superposition (Fig. 3*a*). Residues 6–10 in the Ca^{2+}–B_{12}–BtuB structure shift in position, with a pronounced rotation of residues 6–8. Residues 6 and 7 'flip' or rotate ~180° and remain approximately coplanar with the membrane surface, and the position of the Cα carbon of residue 6 shifts by ~6 Å. The conformational change observed in the Ton box of the Ca^{2+}–B_{12}–BtuB structure does not further extend the Ton box into the periplasmic space (Fig. 3*a,c–f*). The Ton box regions of the SeMet-BtuB and apo BtuB structures are similar to that of the Ca^{2+}–BtuB structure. In pairwise comparisons between SeMet-BtuB, apo BtuB and Ca^{2+}–BtuB structures, the Cα posi-

articles

Fig. 2 Crystallographic structures of BtuB. **a**, apo BtuB; **b**, Ca^{2+}–BtuB; and **c**, Ca^{2+}–B_{12}–BtuB. β-barrel domains are shown in green; hatch domains, in purple. Bound calcium ions are shown in yellow in the Ca^{2+}–BtuB and Ca^{2+}–B_{12}–BtuB structures. The bound cyanocobalamin (vitamin B_{12}) substrate is shown in space-filling representation in the Ca^{2+}–B_{12}–BtuB structure. The left column depicts the structures with extracellular loops pointing upwards and periplasmic turns downwards; the β-strands of the barrel domain span the outer membrane. The right column presents views, normal to the surface of the outer membrane, looking down into the extracellular side of the structures. The hatch domains extend from residues 6–132, with the Ton box located at 6–12. The hatch domain is formed around a core of four β-strands. A short linker (133–136) connects the hatch to the 22-stranded β-barrel domain (137–594). Extracellular loops that are disordered in the apo BtuB structure become partially ordered in the Ca^{2+}–BtuB structure and fully ordered in the Ca^{2+}–B_{12}–BtuB structure. This ordering occurs in the vicinity of the bound calcium ions. Waters, detergent molecules and other (weakly) bound ions are not shown (for clarity).
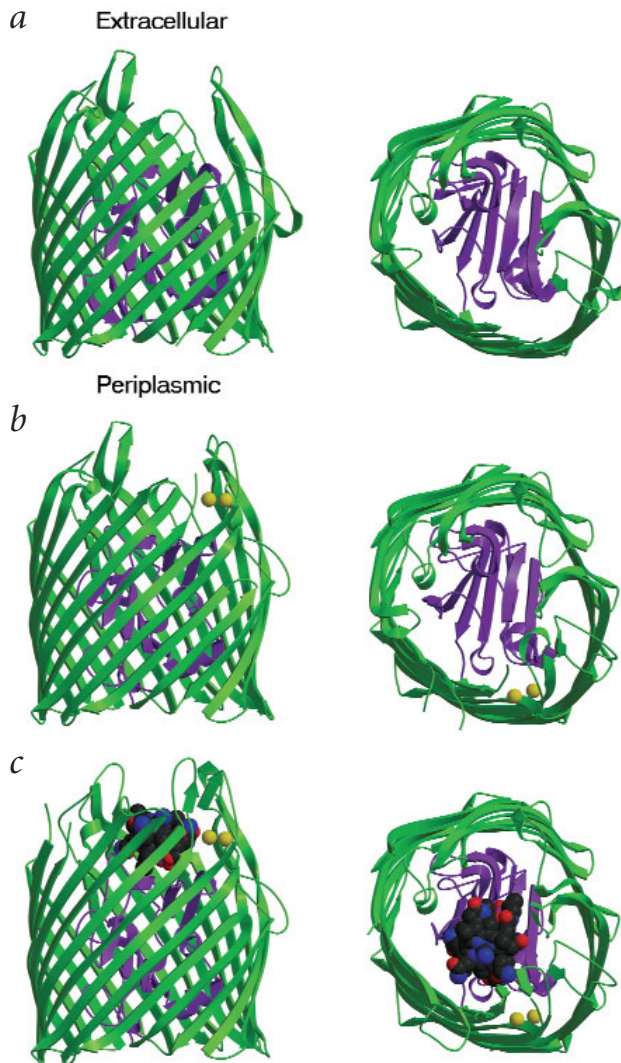
tions of residues 7–12 differ by ~0.2 Å (r.m.s. deviation). However, the Cα positions of these residues in the Ca^{2+}–B_{12}–BtuB structure differ by ~0.6 Å (r.m.s. deviation) with respect to each of the other three structures. Analysis of isotropic *B*-factors indicates that residues 6–8 are more disordered relative to the rest of the protein structure in the Ca^{2+}–B_{12}–BtuB structure but not in the Ca^{2+}–BtuB structure (Fig. 3*b*); this is also seen in comparison of the Ca^{2+}–B_{12}–BtuB structure to the SeMet-BtuB and/or apo BtuB structures (data not shown). Our results are the first direct structural determination of the transmembrane signaling that occurs in the Ton box of a TonB-dependent transporter upon binding of its substrate. This signaling enables recognition of and binding to the transporter by the TonB protein[2–4].

Calcium binding

Anomalous difference Fourier maps, obtained with data collected at the cobalt K-edge (λ = 1.6037 Å) from Ca^{2+}–B_{12}–BtuB crystals, revealed a large (15 σ) peak for the cobalt of the bound cyanocobalamin substrate. Unexpectedly, there were also two other clearly visible peaks (4 σ) in this difference map (Fig. 4*a*). The ratio of peak heights is approximately equal to the ratio of f'' values for cobalt and calcium; thus, we unambiguously assign this doublet of smaller peaks to be calcium ions bound to extracellular loops of BtuB. The SeMet-BtuB and apo BtuB structures possess several disordered extracellular loops. The loops that connect the β-barrel strands 3–4, 5–6 and 7–8 (19, 13 and 11 residues long, respectively) are not seen in the electron density maps. Surprisingly, these loops become partially ordered in the presence of calcium and fully ordered in the presence of calcium and cyanocobalamin (Fig. 4*b–d*).

The two calcium ions, present in both Ca^{2+}–BtuB and Ca^{2+}–B_{12}–BtuB structures, are ~4 Å apart. These calciums are primarily ligated by a five-residue 'aspartate cage' that comprises residues from the ordered extracellular loops connecting β-strands 3–4 and 5–6 of the barrel domain (Fig. 5*a*). Additional ligands consist of a carbonyl in the backbone of residue Tyr229 and, likely, water molecules (not modeled in the current structures because of limited resolution). This aspartate-cage motif is absent from outer membrane iron-siderophore transporters, as assayed by examination of their primary sequences or structures (if known). This distinctive motif of multiple aspartates and/or glutamates coordinating a pair of calcium ions has been observed, however, in other protein structures, among them thermolysin[20], tomato bushy stunt virus coat protein[21], and the pentraxins serum amyloid P pro-

tein[22] and C-reactive protein[23]. We propose that in the absence of calcium, the disordered loops are highly mobile and occlude passage of cobalamin to its binding site. Calcium thus serves to prise open these loops, exposing the high-affinity binding site and permitting facile diffusion of substrate to this site. Analysis of calcium-dependent cobalamin transport in isolated membrane particles led to an estimate for a calcium-binding affinity of ~30 nM (ref. 15); thus, the *in vivo* form of the transporter is likely its calcium-loaded state.

Cyanocobalamin binding

We observe strong electron density for bound cyanocobalamin in $F_o - F_c$ difference maps (Fig. 4*a*). The structure of the cyanocobalamin substrate and its binding site (Fig. 5*b*) shows that two loops of the hatch domain contribute residues that interact with the substrate, with residues 88–92 making the most extensive interaction. Most of the interactions between the BtuB barrel domain and substrate are through the extracellular loops connecting β-strands 5–6 and 7–8; however, the 3–4 loop (ordered by the addition of calcium) does not directly interact with the bound cyanocobalamin. Additional interaction with cyanocobalamin is provided by residues in the loops of β-strands 17–18, 19–20 and 21–22, with the latter two loops contributing aromatic residues. The solvent-accessible
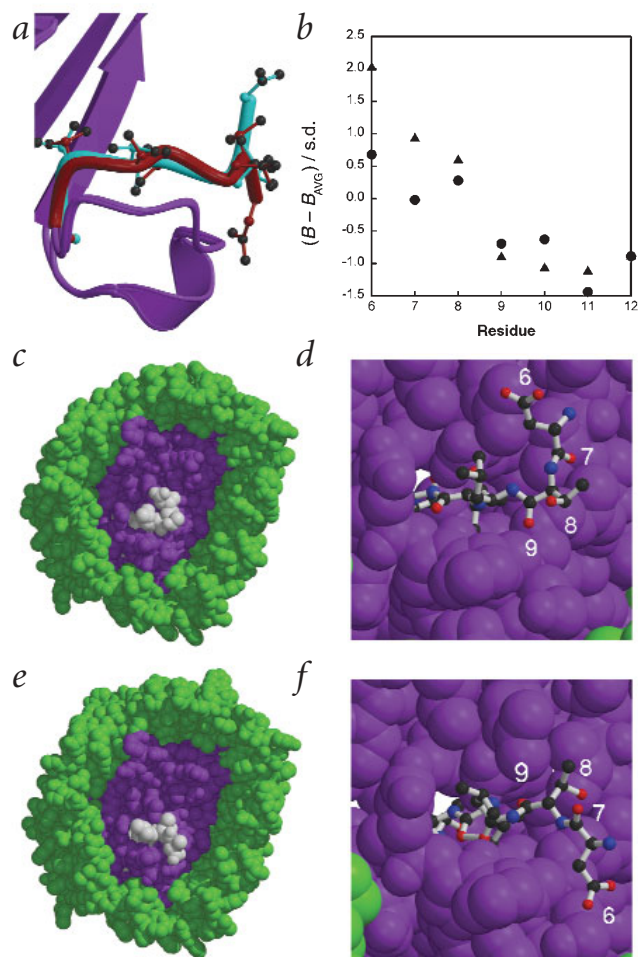
Fig. 3 Substrate-induced conformational change in the Ton box. **a**, Conformation of the Ton box (residues 6–12) in the Ca^{2+}–BtuB (blue) and Ca^{2+}–B$_{12}$–BtuB (red) structures. The backbone of the Ton box is represented as the thick tube with side chains shown as ball-and-stick representation. The Cβ carbons of the side chains are colored identically to the backbone to aid in visualization. The view is from the side, along the periplasmic surface of the outer membrane. **b**, Cα B-factors in the Ton box regions of the Ca^{2+}–BtuB (circles) and Ca^{2+}–B$_{12}$–BtuB (triangles) structures. B_{AVG} and s.d. are the average isotropic B-factor and standard deviation, respectively, of the Cα carbons in the structure (74 ± 16 Å^2 for Ca^{2+}–BtuB, 49 ± 16 Å^2 for Ca^{2+}–B$_{12}$–BtuB). The term $(B - B_{AVG})$ / s.d. indicates the deviation of the B-factor of a residue from that of the average B-factor, normalized by the fluctuation of that average to be in 'standard deviation' units. Isotropic B-factors were calculated from the refined TLS parameters and residual isotropic B-factors with TLSANL[50]. Space-filling representation of Ton box conformation of **c**, Ca^{2+}–BtuB; **d**, Ca^{2+}–BtuB (residues 6–9 labeled); **e**, Ca^{2+}–B$_{12}$–BtuB, and **f**, Ca^{2+}–B$_{12}$–BtuB (residues 6–9 labeled). The hatch domain is colored purple and the barrel domain is colored green. The Ton box (residues 6–12) is colored white in (*c,e*) or rendered as a ball-and-stick represenation in (*d,f*)

surface area of cyanocobalamin decreases by ~900 Å^2 upon binding to BtuB (from 1,243 Å^2 to 347 Å^2), corresponding to an area decrease of 72%. The three loops of BtuB that become ordered in the presence of calcium contribute 125 Å^2 of this binding surface, a modest fraction of the total area. As expected, cyanocobalamin binds in the 'base-on' vitamin conformation, with the N3 nitrogen of the dimethylbenzimidazole group providing the Coα ligand of the corrin ring. The largest structural change in BtuB that occurs upon cyanocobalamin binding is a shift in the position of a loop in the hatch domain (residues 85–96); Cα carbons in these residues shift by as much as 6 Å toward the substrate. Other small conformational changes occur in the extracellular 19–20 loop and the periplasmic 2–3, 8–9 and 10–11 turns. Also, the extracellular loop connecting β-strands 9 and 10 becomes disordered and is not seen in the Ca^{2+}–B$_{12}$–BtuB structure (Fig. 6).

Discussion

Our results are the first direct structural determination of the transmembrane signaling that occurs in the Ton box of a TonB-dependent transporter upon binding of its substrate. Although there is a significant change in the average structure of the Ton box, it does not extend farther out from the hatch domain (Fig. 3*a,c–f*). Thus, it may not be necessary for the Ton box to extend out and away from the hatch domain and into the periplasmic space in order to be recognized by the TonB protein. A significant difference between BtuB and the iron-

siderophore transporters FhuA[10,11] and FecA[13] is the absence of the 'switch helix' of the hatch domain in BtuB. This switch helix, six residues in length and approximately ten residues away from the Ton box, unwinds in the presence of bound substrate. In the crystal structures of FhuA[10,11] and FecA[13], Cα carbons of the switch helix move as much as 15 Å or more following this conformational transition. By sequence analysis and by direct structural inspection, neither BtuB nor FepA[12] possesses this switch helix. Thus, at least in these two cases, an unwinding switch helix is inessential for function. A structure of FhuA, in complex with a rifamycin-derivative antibiotic that it transports, shows a more disordered, but not unwound, switch helix[24], implying that this unfolding transition may not be obligate for its function.

We observe a substrate-induced conformational change in the Ton box region of BtuB. Previous studies, using other experimental techniques, have also probed the structure and dynamics of the Ton box of BtuB and characterized changes in experimental observables upon substrate binding[25,26]. These studies used scanning cysteine mutagenesis, either for observation of disulfide crosslinking with TonB[25] or for EPR spectroscopy of spin-probe–labeled cysteine mutants[26]. Inspection of the Ton box regions of our structures indicates that several residues (residues 9, 11 and 12) are tightly packed against other portions of BtuB. We suggest that mutation of residues at these positions to residues (or spin-labeled residues) with bulkier side chains than those of wild type may destabilize or otherwise perturb the wild type structure and/or dynamics of BtuB during its transport cycle. The other residues of the Ton box have less severe steric constraints and, thus, are likely to be less perturbed by mutagenesis and labeling. The disulfide crosslinking study[25] indicates that increased disulfide formation occurs between TonB and residues 8, 10 and 12. Accessibility of residues 8 and 10 to crosslinking and interaction with TonB is certainly plausible based on our structures (Fig. 3*d,f*); we would suggest that substitution of a cysteine for the smaller wild type Ala at position 12 may be perturbative. The EPR study[26] indicates that all residues of the Ton box (6–12) become more disordered upon substrate binding. Increasing disorder of residues 6–8 is consistent with our observation of an increase in relative B-factor at these positions (Fig. 3*b*). We would suggest that introduction of spin labels at positions 9, 11 and 12 may be perturbative. Residue 10, with a reduced but non-zero solvent accessibility, may or may not be perturbed by addition of the spin probe. A recent paper[27] presents data on possible perturbative effects of spin probes on Ton

Fig. 4 Experimental determination of bound cyanocobalamin and calcium, and their effects upon BtuB structure **a**, Electron density depicting the location of cyanocobalamin and calcium in the Ca^{2+}–B_{12}–BtuB structure. Anomalous difference density indicates the location of the cobalt of cyanocobalamin (red, 15 σ) and the location of two bound calcium ions (blue, 4 σ). σ_A^{42}-weighted $F_o - F_c$ difference density (brown, 3 σ) indicates the location of the bound substrate. Portions of the barrel have been removed for clarity. Surface representations of BtuB. **b**, apo BtuB; **c**, Ca^{2+}–BtuB; and **d**, Ca^{2+}–B_{12}–BtuB. The view is normal to the surface of the outer membrane, looking down onto the extracellular side. Loops that change their state of ordering are indicated in green. The extracellular loop connecting β-strands 9–10 is ordered in the apo BtuB and Ca^{2+}–BtuB structures. The addition of calcium causes a partial ordering of the extracellular loops connecting β-strands 3–4, 5–6 and 7–8. The ordering of these three loops is complete in the Ca^{2+}–B_{12}–BtuB structure. Bound cyanocobalamin is indicated in red in (**d**).
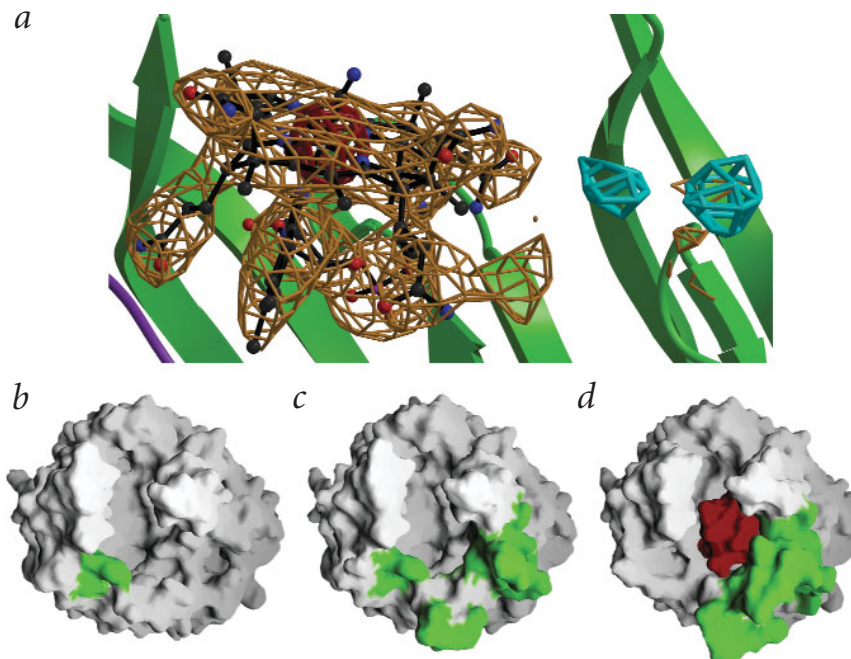
box structure and behavior. This study, a follow-up of previous EPR investigations of Ton box structure and dynamics[26], used double-labeling and phenylalanine-scanning mutagenesis to probe the effects of bulky substituents in the Ton box. A conclusion of this paper is that the lineshape and mobility observed for the Ton box spin-labeled at position 11 (and possibly at position 12) may be an artifact of spin label incorporation[27]. To address these issues comprehensively, we have an effort underway to produce and crystallize spin-labeled cysteine mutants of BtuB. Crystals of spin-labeled protein can be used for both structure determination and EPR, as was demonstrated for the soluble protein T4 lysozyme[28].

The structure of the iron-siderophore transporter FecA with its bound dinuclear citrate substrate indicates a sequestration of the substrate within the barrel as the extracellular loops fold over and shield the substrate from the extracellular milieu[13]. The possibility of exclusion of substrate from the extracellular compartment as a step during a TonB-dependent outer membrane transport cycle is intriguing. We examined whether this occurred in the Ca^{2+}–B_{12}–BtuB structure and found that it does not. The 'upper' extracellular-facing surface of cyanocobalamin remains exposed when bound to BtuB. Examination of crystal packing of the complex indicates that five extracellular loops (3–4, 5–6, 15–16, 17–18 and 19–20) participate in crystal contacts. These loops are approximately contiguous and lie on roughly one-half of the circumference of the extracellular-facing 'top' of the barrel domain of BtuB. It is possible that crystal packing may hinder or restrict some movement of one or more of these loops. However, none of the extracellular loops of the other half of the barrel domain participate in crystal contacts, and the substrate is not covered by the loops of this portion of the barrel. We posit that sequestration of the substrate is a geometrical (or stereochemical) consequence of the specific transporter and substrate. In BtuB, the cyanocobalamin substrate is large (larger than any iron-siderophore substrate in existing structures), and the extracellular loops of the barrel domain are small (smaller than those of iron-siderophore transporters). Thus, in the case of BtuB, the substrate is not excluded from the extracellular space when bound in its initial energy-independent fashion. By contrast, the FecA substrate is small, and the FecA extracellular barrel loops are large; hence, sequestration is both possible and observed in the structure of the complex[13]. Even though complete parti-
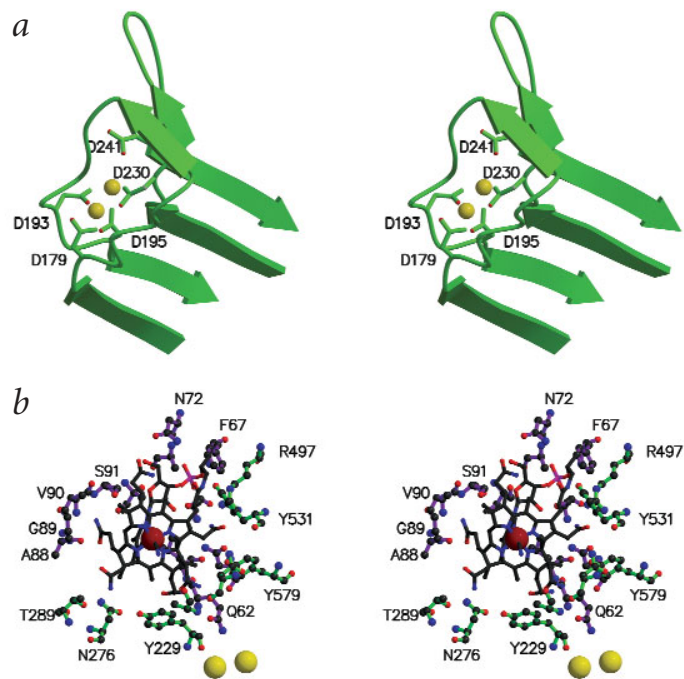

Fig. 5 Calcium and cyanocobalamin binding in BtuB **a**, Stereo view of the 'aspartate cage' binding the two calcium ions (yellow) in the Ca^{2+}–BtuB and Ca^{2+}–B_{12}–BtuB structures. **b**, Stereo view of cyanocobalamin bound to BtuB. The view is normal to the surface of the outer membrane, looking down into the extracellular side. Residues within 4.5 Å of the substrate are shown, with those of the hatch domain colored purple and those from the barrel colored green. The calcium ions are included to indicate the orientation of the molecule (which is the same as that of Fig. 1).

Fig. 6 Structural differences between the apo BtuB, Ca^{2+}–BtuB and Ca^{2+}–B_{12}–BtuB structures. **a**, Schematic diagram summarizing the changes in the BtuB structure upon addition of calcium, or calcium and cyanocobalamin. **b**, R.m.s. differences of $C\alpha$ position between apo BtuB and Ca^{2+}–BtuB structures (average r.m.s = 0.2 Å), and between Ca^{2+}–BtuB and Ca^{2+}–B_{12}–BtuB structures (average r.m.s = 0.4 Å). Significantly more and larger magnitude structural changes occur with addition of cyanocobalamin and calcium *versus* addition of calcium alone.
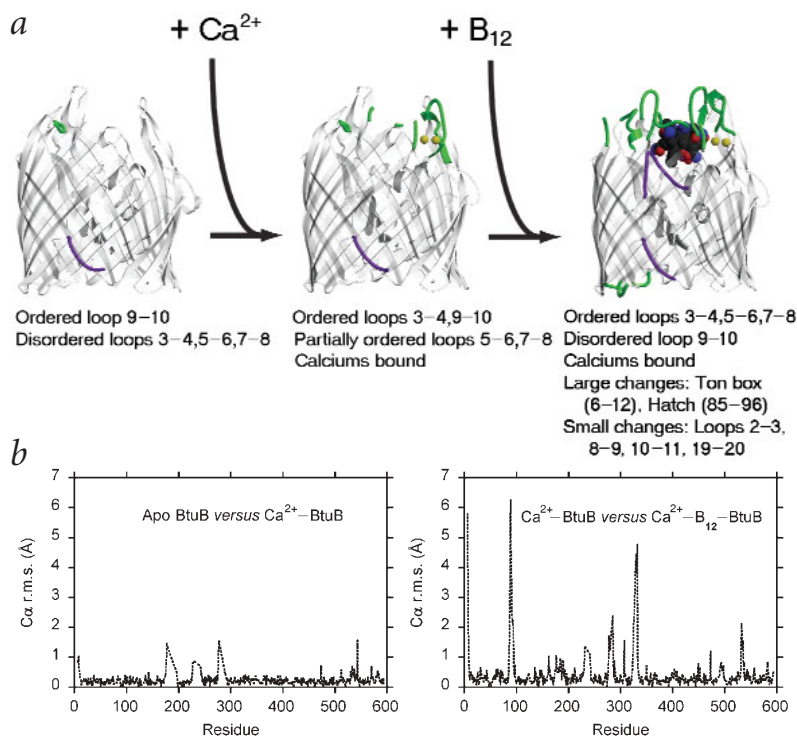
tioning of substrate away from the extracellular compartment may not occur in all TonB-dependent outer membrane transporters, other changes in the conformation and dynamics of extracellular loops upon substrate binding may play significant roles in the transport cycle. Structural comparisons of the four structures solved thus far indicate that, although all TonB-dependent outer membrane transporters may possess similar structural and functional archetypes, substantial variation exists between them.

In a current paradigm for the TonB-dependent outer-membrane transport cycle, energy-independent substrate binding at the extracellular side of the transporter induces a transmembrane signaling event that causes a conformational change in the portion of the transporter facing out into the periplasmic space. This conformational change increases the affinity of TonB for the transporter and enables coupling of TonB to the transporter. Biochemical studies indicate that a stable complex can be formed in solution between a TonB domain and FhuA in the presence of its substrate ferricrocin, although this complex is not formed in the absence of substrate[29]. This result indicates that substrate-induced conformational change and increased affinity of the transporter for TonB is energy independent. The coupling between transporter and TonB enables the energy-dependent step of the transport cycle in which the transporter is perturbed in some way that enables the substrate to leave its binding site and traverse the lumen of the barrel domain. This step (whose structural nature is currently unknown) involves a change to the hatch domain — such as shifting it, unfolding it or removing it from the barrel — so that it does not occlude the barrel.

An additional key mechanistic question that remains unanswered is the manner in which TonB-dependent transport proceeds vectorially. Even if (somehow) the hatch is removed from the barrel, the bound substrate must transit through the barrel to the periplasmic side of the outer membrane. Biochemical studies of the isolated hatch domain of FepA indicate that, outside of the environs of the barrel, it is unfolded but still able to bind its substrate, although at lower affinity than in the intact transporter[30]. Alternatively or additionally, the periplasmic binding protein (for BtuB, this protein is BtuF[19,31]) that conveys substrate across the periplasmic space to its inner membrane transporter may possibly interact with the outer membrane transporter in this vectorial process. Clearly, fundamental mechanistic questions remain unanswered for TonB-depen-

Table 1 Data collection, phasing and refinement statistics				
Structure	SeMet-BtuB	Apo BtuB	Ca^{2+}–BtuB	Ca^{2+}–B_{12}–BtuB
Beamline	APS SBC 19-ID	CHESS F1	APS IMCA 17-ID	NSLS X25
Wavelength (Å)	0.9787	0.9000	1.255	1.6037
Resolution range[1]	20.0–2.7	25.0–2.0	20.0–3.3	20.0–3.1
	(2.78–2.70)	(2.18–2.00)	(3.33–3.30)	(3.21–3.10)
Unique reflections	24,020	55,620	13,146	16,612
Redundancy[2]	6.0	8.9	9.7	5.8
Completeness (%)[1]	96.4 (89.3)	99.6 (97.8)	95.6 (95.8)	100.0 (99.7)
R_{sym} (%)[1,3]	9.1 (56.0)	6.5 (41.2)	7.9 (22.0)	7.3 (35.0)
Phasing power	1.67			
Figure of merit				
SAD	0.202			
DM	0.840			
R-factor[4]	24.4	19.4	23.4	22.4
R_{free}[5]	28.6	23.2	25.9	26.0
R.m.s. deviation				
Bond lengths (Å)	0.018	0.021	0.028	0.032
Angles (°)	2.12	1.95	2.62	3.13
Number of atoms				
Protein	4,512	4,742	4,685	4,853
Water	82	235	0	0
Other	C8E4[6] (6)	C8E4 (7), Mg	C8E4 (6), Ca (4)	C8E4 (6), Ca (2), B_{12}

[1]Number in parentheses is for the highest shell.
[2]For the SeMet-BtuB and Ca^{2+}–B_{12}–BtuB datasets, redundancy is calculated without merging the Friedel mates.
[3]$R_{sym} = \Sigma|I_{hkl} - <I>| / \Sigma(I_{hkl})$, where I_{hkl} is the integrated intensity of a given reflection.
[4]R-factor = $(\Sigma|F_o - F_c|) / (\Sigma F_o)$, where F_o and F_c are observed and calculated structure factors, respectively.
[5]A test set of 5% of the observed reflections was used to calculate the R_{free} (ref. 51) in all structures.
[6]C8E4: *N*-octyl tetraoxyethylene.

dent outer-membrane transport. A unified approach involving structural, spectroscopic, biochemical and other approaches will be required to further dissect this active transport system.

Methods

Expression, purification, and crystallization. Expression, purification, crystallization, substrate-soaking and crystal cryomounting of BtuB were done as described[32]. The crystals are in space group $P3_121$, with a monomer in the asymmetric unit and a solvent content of ~60%. Two useful crystal forms are obtained. The short-c variant ($a = b = 81.6$ Å, $c = 210.0$ Å, $\alpha = \beta = 90°$ and $\gamma = 120°$) was used to solve the apo BtuB structure. The more prevalent long-c variant ($a = b = 81.6$ Å, $c = 226–227$ Å, $\alpha = \beta = 90°$ and $\gamma = 120°$) was used to solve the SeMet-BtuB, Ca^{2+}–BtuB and Ca^{2+}–B_{12}–BtuB structures.

Structure determination. All diffraction data were processed with HKL2000 (ref. 33). The SeMet-BtuB structure was solved by SAD and density modification. All eight selenium sites were independently located by either SnB[34] or the heavy_search routine[35] of CNS[36]. Selenium positions were refined, and SAD phases were calculated with SHARP[37]; solvent-based density modification was performed with SOLOMON[38] as implemented within SHARP. Model building was done using O[39] and Quanta (Accelrys). Structure refinement was performed with REFMAC[40] with inclusion of TLS refinement[41]. σ_A[42]-weighted difference maps and prime_and_switch phased maps[43] were used in rebuilding cycles. The apo BtuB structure was solved by molecular replacement with a search model derived from the SeMet-BtuB structure. Solvent molecules were added using X-SOLVATE (Accelrys). SAD data was collected at the Co K-edge from the Ca^{2+}–B12–BtuB crystal. Molecular replacement with the apo BtuB structure yielded initial phases that were used to calculate anomalous difference Fourier maps for determination of the initial positions of bound cobalt and calcium. This SAD data was used as input into SHARP for SAD phasing, which included phase combination with the initial molecular replacement phases and subsequent density modification. The small contribution of the cobalt (and calcium) anomalous signals to the molecular replacement phases was useful for obtaining the best-quality electron density maps. Finally, the Ca^{2+}–BtuB structure was solved by molecular replacement. All molecular replacement calculations were performed with AMoRe[44], and other computation used various programs from the CCP4 suite[45]. Crystallographic statistics are summarized in Table 1.

Coordinates. Coordinates and structure factors have been deposited with the Protein Data Bank (accession codes 1NQF (SeMet-BtuB), 1NQE (apo BtuB), 1NQG (Ca^{2+}–BtuB) and 1NQH (Ca^{2+}–B_{12}–BtuB)).

Competing interests statement

The authors declare that they have no competing financial interests.

1. Postle, K. Active transport by customized β-barrels. *Nat. Struct. Biol.* **6**, 3–6 (1999).

2. Kadner, R.J. Vitamin B_{12} transport in *Escherichia coli*: energy coupling between membranes. *Mol. Microbiol.* **4**, 2027–2033 (1990).

3. Postle, K. TonB protein and energy transduction between membranes. *J. Bioenerg. Biomembr.* **25**, 591–601 (1993).

4. Braun, V. Energy-coupled transport and signal transduction through the Gram-negative outer membrane *via* TonB-ExbB-ExbD–dependent receptor proteins. *FEMS Microbiol. Rev.* **16**, 295–307 (1995).

5. Lundrigan, M.D. & Kadner, R.J. Nucleotide sequence of the gene for the ferrienterochelin receptor FepA in *Escherichia coli*. Homology among outer membrane receptors that interact with TonB. *J. Biol. Chem.* **261**, 10797–10801 (1986).

6. Schramm, E., Mende, J., Braun, V. & Kamp, R.M. Nucleotide sequence of the colicin B activity gene *cba*: consensus pentapeptide among TonB-dependent colicins and receptors. *J. Bacteriol.* **169**, 3350–3357 (1987).

7. Heller, K., Mann, B.J. & Kadner, R.J. Cloning and expression of the gene for the vitamin B_{12} receptor protein in the outer membrane of *Escherichia coli*. *J. Bacteriol.* **161**, 896–903 (1985).

8. Schoffler, H. & Braun, V. Transport across the outer membrane of *Escherichia coli* K12 *via* the FhuA receptor is regulated by the TonB protein of the cytoplasmic membrane. *Mol. Gen. Genet.* **217**, 378–383 (1989).

9. Larsen, R.A., Foster-Hartnett, D., McIntosh, M.A. & Postle, K. Regions of *Escherichia coli* TonB and FepA proteins essential for *in vivo* physical interactions. *J. Bacteriol.* **179**, 3213–3221 (1997).

10. Locher, K.P. *et al*. Transmembrane signaling across the ligand-gated FhuA receptor: crystal structures of free and ferrichrome-bound states reveal allosteric changes. *Cell* **95**, 771–778 (1998).

11. Ferguson, A.D., Hofmann, E., Coulton, J.W., Diederichs, K. & Welte, W. Siderophore-mediated iron transport: crystal structure of FhuA with bound lipopolysaccharide. *Science* **282**, 2215–2220 (1998).

12. Buchanan, S.K. *et al*. Crystal structure of the outer membrane active transporter FepA from *Escherichia coli*. *Nat. Struct. Biol.* **6**, 56–62 (1999).

13. Ferguson, A.D. *et al*. Structural basis of gating by the outer membrane transporter FecA. *Science* **295**, 1715–1719 (2002).

14. Roth, J.R., Lawrence, J.G. & Bobik, T.A. Cobalamin (coenzyme B_{12}): synthesis and biological significance. *Annu. Rev. Microbiol.* **50**, 137–181 (1996).

15. Bradbeer, C., Reynolds, P.R., Bauler, G.M. & Fernandez, M.T. A requirement for calcium in the transport of cobalamin across the outer membrane of *Escherichia coli*. *J. Biol. Chem.* **261**, 2520–2523 (1986).

16. Di Masi, D.R., White, J.C., Schnaitman, C.A. & Bradbeer, C. Transport of vitamin B_{12} in *Escherichia coli*: common receptor sites for vitamin B_{12} and the E colicins on the outer membrane of the cell envelope. *J. Bacteriol.* **115**, 506–513 (1973).

17. Bradbeer, C., Woodrow, M.L. & Khalifah, L.I. Transport of vitamin B_{12} in *Escherichia coli*: common receptor system for vitamin B_{12} and bacteriophage BF23 on the outer membrane of the cell envelope. *J. Bacteriol.* **125**, 1032–1039 (1976).

18. Locher, K.P., Lee, A.T. & Rees, D.C. The *E. coli* BtuCD structure: a framework for ABC transporter architecture and mechanism. *Science* **296**, 1091–1098 (2002).

19. Borths, E.L., Locher, K.P., Lee, A.T. & Rees, D.C. The structure of *Esherichia coli* BtuF and binding to its cognate ATP binding cassette transporter. *Proc. Natl. Acad. Sci. USA* **99**, 16642–16647 (2002).

20. Matthews, B.W. *et al*. Structure of thermolysin. *Nat. New Biol.* **238**, 41–43 (1972).

21. Hogle, J., Kirchhausen, T. & Harrison, S.C. Divalent cation sites in tomato bushy stunt virus: difference maps at 2.9 Å resolution. *J. Mol. Biol.* **171**, 95–100 (1983).

22. Emsley, J. *et al*. Structure of pentameric human serum amyloid P component. *Nature* **367**, 338–345 (1994).

23. Shrive, A.K. *et al*. Three dimensional structure of human C-reactive protein. *Nat. Struct. Biol.* **3**, 346–353 (1996).

24. Ferguson, A.D. *et al*. Active transport of an antibiotic rifamycin derivative by the outer-membrane protein FhuA. *Structure* **9**, 707–716 (2001).

25. Cadieux, N. & Kadner, R.J. Site-directed disulfide bonding reveals an interaction site between energy-coupling protein TonB and BtuB, the outer membrane cobalamin transporter. *Proc. Natl. Acad. Sci. USA* **96**, 10673–10678 (1999).

26. Merianos, H.J., Cadieux, N., Lin, C.H., Kadner, R.J. & Cafiso, D.S. Substrate-induced exposure of an energy-coupling motif of a membrane transporter. *Nat. Struct. Biol.* **7**, 205–209 (2000).

27. Fanucci, G.E. *et al*. Substrate-induced conformational changes of the periplasmic N-terminus of an outer-membrane transporter by site-directed spin labelling. *Biochemistry* **42**, 1391–1400 (2003).

28. Langen, R., Oh, K.J., Cascio, D. & Hubbell, W.L. Crystal structures of spin-labelled T4 lysozyme mutants: implications for the interpretation of EPR spectra in terms of structure. *Biochemistry* **39**, 8396–8405 (2000).

29. Moeck, G.S. & Letellier, L. Characterization of in vitro interactions between a truncated TonB protein from *Escherichia coli* and the outer membrane receptors FhuA and FepA. *J. Bacteriol.* **183**, 2755–2764 (2001).

30. Usher, K.C., Özkan, E., Gardner, K.H. & Deisenhofer, J. The plug domain of FepA, a TonB-dependent transport protein from *Escherichia coli*, binds its siderophore in the absence of the transmembrane barrel domain. *Proc. Natl. Acad. Sci. USA* **98**, 10676–10681 (2001).

31. Cadieux, N. *et al*. Identification of the periplasmic cobalamin-binding protein BtuF of *Escherichia coli*. *J. Bacteriol.* **184**, 706–717 (2002).

32. Chimento, D.P., Mohanty, A.K., Kadner, R.J. & Wiener, M.C. Crystallization and preliminary X-ray crystallographic analysis of the *Escherichia coli* outer membrane cobalamin transporter BtuB. *Acta Crystallogr. D* **59**, 509–511 (2003).

33. Otwinowski, Z. & Minor, W. Processing of X-ray diffraction collected in oscillation mode. *Methods Enzymol.* **276**, 307–326 (1997).

34. Miller, R. & Gallo, S.M. SnB: crystal structure determination *via* Shake-and-Bake. *J. Appl. Crystallogr.* **27**, 613–621 (1994).

35. Grosse-Kuntsleve, R.W. & Brunger, A.T. A highly automated heavy-atom search procedure for macromolecular structures. *Acta Crystallogr. D* **55**, 1568–1577 (1999).

36. Brunger, A.T. *et al*. Crystallography & NMR System: a new software suite for macromolecular structure determination. *Acta Crystallogr. D* **54**, 905–921 (1998).

37. de La Fortelle, E. & Bricogne, G. SHARP: maximum-likelihood heavy-atom parameter refinement for multiple isomorphous replacement and multiwavelength anomalous diffraction methods. *Methods Enzymol.* **176**, 472–494 (1997).

38. Abrahams, J.P. & Leslie, A.G.W. Methods used in the structure determination of bovine mitochondrial F-1 ATPase. *Acta Crystallogr. D* **52**, 30–42 (1996).

39. Jones, T.A., Zou, J.Y., Cowan, S.W. & Kjeldgaard, M. Improved methods for building protein models in electron density maps and the location of errors in these models. *Acta Crystallogr. A* **47**, 110–119 (1991).

40. Murshudov, G.N., Vagin, A.A. & Dodson, E.J. Refinement of macromolecular structure by the maximum-likelihood method. *Acta Crystallogr. D* **53**, 240–255 (1997).

41. Winn, M.D., Isupov, M.N. & Nurshudov, G.N. Use of TLS parameters to model anisotropic displacements in macromolecular refinement. *Acta Crystallogr. D* **57**, 122–133 (2001).

42. Read, R.J. Improved Fourier coefficients for maps using phases from partial structures with errors. *Acta Crystallogr. A* **42**, 140–149 (1986).

43. Terwilliger, T.C. Map-likelihood phasing. *Acta Crystallogr. D* **57**, 1763–1775 (2001).

44. Navaza, J. Implementation of molecular replacement in AMoRe. *Acta Crystallogr. D* **57**, 1367–1372 (2001).

45. Collaborative Computational Project, Number 4. The CCP4 suite: programs for protein crystallography. *Acta Crystallogr. D* **50**, 760–763 (1994).

46. Kraulis, P. MOLSCRIPT: a program to produce both detailed and schematic plots of protein structures. *J. Appl. Crystallogr.* **24**, 946–950 (1991).

47. Esnouf, R.M. An extensively modified version of MolScript that includes greatly enhanced coloring capabilities. *J. Mol. Graph.* **15**, 132–134 (1997).

48. Merrit, E. & Murphy, M. Raster3D version 2.0. A program for photorealistic molecular graphics. *Acta Crystallogr. D* **50**, 869–873 (1994).

49. Nicholls, A., Bharadwaj, R. & Honig, B. GRASP: graphical representation and analysis of surface properties. *Biophys. J.* **64**, 166–170 (1993).

50. Howlin, B., Butler, S.A., Moss, D.S., Harris, G.W. & Driessen, H.P.C. TLSANL: TLS parameter analysis program for segmented anisotropic refinement of macromolecular structures. *J. Appl. Crystallogr.* **26**, 622–624 (1993).

51. Brunger, A.T. The free R value: a novel statistical quantity for assessing the accuracy of crystal structures. *Nature* **355**, 472–474 (1992).